Initial-state fluctuations from midperipheral to ultracentral collisions in an event-by-event transport approach

S. Plumari, G. L. Guardo, F. Scardina, and V. Greco
Department of Physics and Astronomy, University of Catania, Via S. Sofia 64, I-95125 Catania, Italy
and INFN-Laboratori Nazionali del Sud, Via S. Sofia 62, I-95123 Catania, Italy
(Received 28 July 2015; revised manuscript received 24 September 2015; published 5 November 2015)

We have developed a relativistic kinetic transport approach that incorporates initial-state fluctuations allowing to study the buildup of elliptic flow v_2 and high-order harmonics v_3, v_4, and v_5 for a fluid at fixed $\eta/s(T)$. We study the effect of the η/s ratio and its T dependence on the buildup of the $v_n(p_T)$ for two different beam energies: RHIC for Au+Au at $\sqrt{s} = 200$ GeV and LHC for Pb + Pb at $\sqrt{s} = 2.76$ TeV. We find that for the two different beam energies considered the suppression of the $v_n(p_T)$ due to the viscosity of the medium have different contributions coming from the crossover or QGP phase. Our study reveals that only in ultracentral collisions (0–0.2%) the $v_n(p_T)$ have a stronger sensitivity to the T dependence of η/s in the QGP phase and this sensitivity increases with the order of the harmonic n. Moreover, the study of the correlations between the initial spatial anisotropies ϵ_n and the final flow coefficients v_n shows that at LHC energies there is more correlation than at RHIC energies. The degree of correlation increases from peripheral to central collisions, but only in ultracentral collisions at LHC, we find that the linear correlation coefficient $C(n,n) \approx 1$ for $n = 2,3,4$, and 5. This suggests that the final correlations in the (v_n, v_m) space reflect the initial correlations in the (ϵ_n, ϵ_m) space.

DOI: 10.1103/PhysRevC.92.054902 PACS number(s): 25.75.Ld, 12.38.Aw, 12.38.Mh

I. INTRODUCTION

The experimental results accumulated in these years in the ultrarelativistic heavy-ion collisions (uRHICs), first in the experiments conducted at RHIC and more recently at the LHC, has shown that the elliptic flow $v_2 = \langle \cos(2\varphi_p) \rangle = \langle (p_x^2 - p_y^2)/(p_x^2 + p_y^2) \rangle$ is the largest ever observed in HIC [1,2]. The elliptic flow is a measurement of the momentum anisotropy of the emitted particles and it is an observable that encodes information about the transport properties of the matter created in these collisions. Theoretical calculations within viscous hydrodynamics [3,4], and in recent years also calculations performed within transport approach [5–7], have shown that this large value of v_2 is consistent with a matter with a very low shear viscosity to entropy density ratio η/s close to the conjectured lower bound for a strongly interacting system, $\eta/s = 1/4\pi$ [8].

While early studies have been focused on elliptic flow generated by the global almond shape of the fireball for noncentral collisions, in recent years the possibility to measure experimentally the event-by-event angular distribution of emitted particle has made it possible to go beyond such a simplified picture, accessing the fluctuating shape that encodes higher-order harmonics generating nonzero flows $v_n = \langle \cos(n\,\varphi_p) \rangle$ [9–11]. Hence most of the research activity has been now focused on the study of the effects of the fluctuations in the initial geometry due to the fluctuations of the position of the nucleons in the overlap region of the collision [12–17]. Such fluctuations in the initial geometry are sources for momentum anisotropies of any nth order harmonics $v_n = \langle \cos(n\,\varphi_p) \rangle$ and in particular of the triangular flow $n = 3$, that especially in ultracentral collisions appears as the largest one [11,18,19].

The comparison between event-by-event viscous hydrodynamical calculations and the experimental results for v_n seems to confirm a finite but not too large value of $4\pi\eta/s \sim 1 - 3$ [15,16]. However, small values of η/s is not an evidence of the creation of a QGP phase. A phenomenological estimation of its temperature dependence could give information if the matter created in these collisions undergoes a phase transition [20–22]. Information about a temperature dependence of η/s can be achieved studying the $v_2(p_T)$ and the high order harmonic $v_n(p_T)$ in a wider range of energies. Similar studies have been performed using a transport approach but only for the elliptic flow in an approach not incorporating event-by-event fluctuations [22,23]. In this paper we extend this analysis to high order harmonics studying the role of the η/s on the buildup of $v_n(p_T)$ using for the first time a cascade approach with initial-state fluctuations.

There are several theoretical indications that η/s should have a particular behavior with the temperature [20,21,24–27]. As an example in Fig. 1 it is shown a collection of theoretical results about the temperature dependence of η/s. Figure 1 shows that in general η/s should have a typical behavior of phase transition with a minimum close to the critical temperature T_C [20–23].

On one hand at low-temperature estimates of η/s in the chiral perturbation theory for a meson gas [24,25], have shown that in general η/s is a decreasing function with the temperature, see down triangles in Fig. 1. Similar results for η/s have been extrapolated from heavy-ion collisions at intermediate energies, see HIC-IE diamonds in Fig. 1. On the other hand at higher temperature $T > T_c$ lQCD calculations have shown that in general η/s becomes an increasing function with the temperature [26,29], see up triangles and circles in Fig. 1, but due to the large error bars in the lQCD results for η/s it is not possible to infer a clear temperature dependence in the QGP phase. The analysis at different energies of $v_2(p_T)$ and the extension to high order harmonics $v_n(p_T)$ can give further information about the T dependence of η/s. In this

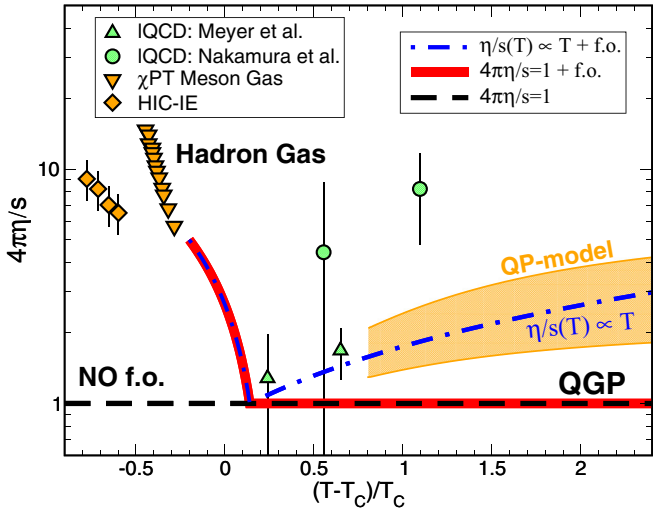

FIG. 1. (Color online) Different parametrizations for η/s as a function of the temperature. The orange area refers to the quasiparticle model predictions for η/s [28]. The three different lines indicate different possible T dependencies studied in this paper. Symbols are as in the legend. See the text for more details.

paper we study and discuss the buildup of anisotropic flows v_n in ultrarelativistic HIC treating the system as a fluid with some $\eta/s(T)$. This is achieved by mean of a transport approach with initial-state fluctuations. The paper is organized as follows. In Sec. II, we introduce the transport approach at fixed shear viscosity to entropy density η/s. In Sec. III, we discuss the initial conditions and in particular the implementation of the initial-state fluctuations in the transport approach. In Sec. IV, we study the time evolution of the anisotropic flows $\langle v_n\rangle$ and the effect of the $\eta/s(T)$ on the differential $v_n(p_T)$. Finally, in Sec. V we study the correlations between the initial asymmetry in coordinate space measured by the coefficients ϵ_n and the final anisotropy in momentum space measured by the anisotropic flows $\langle v_n\rangle$. In this paper we will show results on $v_n(p_T)$ for $n = 2,3,4$, and 5 for the two different systems Au + Au at $\sqrt{s} = 200$ GeV and Pb + Pb at $\sqrt{s} = 2.76$ TeV at different centralities.

II. KINETIC APPROACH AT FIXED SHEAR VISCOSITY TO ENTROPY DENSITY RATIO

In this work we employ the kinetic transport theory to study the evolution of the fireball created in relativistic heavy-ion collisions. We perform such simulations using a relativistic transport code developed to perform studies of the dynamics of heavy-ion collisions at both RHIC and LHC energies [5,7,30–33]. The evolution of the phase-space distribution function $f(x,p,t)$ is given by solving the relativistic Boltzmann transport (RBT) equation:

$$p^\mu\, \partial_\mu f(x,p) = C[f] + S[f_0], \tag{1}$$

where $C[f]$ is the Boltzmann-like collision integral. In the result shown in this paper we have considered only the $2 \leftrightarrow 2$ processes and for one-component system $C[f]$ can be written as,

$$C[f] = \int_{2,1',2'} (f_{1'} f_{2'} - f f_2)|\mathcal{M}|^2 \delta^4(p + p_2 - p_{1'} - p_{2'}), \tag{2}$$

where $\int_{2,1',2'} = \int \Pi_{k=2,1',2'} d^3p_k/2E_k(2\pi)^3$ and $\mathcal{M}$ denotes the transition amplitude for the elastic processes, which is directly linked to the differential cross section $|\mathcal{M}|^2 = 16\pi\, s\,(s - 4M^2) d\sigma/dt$ with s the Mandelstam invariant. Numerically, we solve the RBT equation using the so-called test particle method and the collision integral is solved by using Monte Carlo methods based on the stochastic interpretation of transition amplitude [5,31,34].

In the standard use of the transport theory one fixes the microscopical details of the scatteringlike matrix element or cross sections of the processes to study the effect of the microscopical details on the observables. This is however not our aim; we exploit the cross section $\sigma_{\rm tot}$ as a tool to determine the η/s of the system. As shown in Ref. [35] in the hydrodynamic limit observables such as $v_2(p_T)$ or spectra don't depend on the microscopic details encoded in $|\mathcal{M}|^2$, in agreement with the implicit assumption of hydrodynamics. In such an approach it is possible to study directly the impact of η/s on observables such as the anisotropic flows $v_n(p_T)$, which is the main focus of this paper. Compared with the viscous hydrodynamic calculations, a kinetic approach at fixed η/s has manly two advantages: first, in this approach we start from a description in terms of $f(x,p)$ instead of starting from $T^{\mu\nu}(x)$ and it is possible to include initial nonequilibrium effects (see Refs. [32,33]). Second, this approach is not based on an ansatz for the viscous corrections for the phase-space distribution function δf with the limitation in the transverse momentum range in order to ensure that $\delta f/f \ll 1$. Also this approach provides a tool to study the effect of η/s on the observables in a wider range of η/s and in transverse momentum p_T. Notice also that the kinetic freeze out can be determined self-consistently with an increasing $\eta/s(T)$ that determines a smooth switching off of the scattering rates. A more detailed discussion can be found in previous papers, see Refs. [5,32,33]. The disadvantage of the present approach is that hadronization has not yet been included. A more general disadvantage is that RBT converge to viscous hydrodynamics with the relaxation time typical of a kinetic theory. However, viscous hydrodynamics with relaxation times of kinetic theory have been shown to be in quite good agreement with experimental data.

In order to study the dynamical evolution of the fireball with a certain $\eta/s(T)$ we determine locally in space and time the total cross section $\sigma_{\rm tot}$ needed to have the wanted local viscosity. As shown in Ref. [31] the Chapmann-Enskog theory correctly describes the relation between $\eta \leftrightarrow T, \sigma(\theta), \rho$ providing a good agreement with the results obtained using the Green-Kubo correlator. In the Chapmann-Enskog theory and for a pQCD inspired cross section, typically used in parton cascade approaches [5,6,34,36–39], $d\sigma/dt \sim \alpha_s^2/(t - m_D^2)^2$, the η/s is given by the following expression:

$$\eta/s = \frac{1}{15}\langle p\rangle\, \tau_\eta = \frac{1}{15}\frac{\langle p\rangle}{g(a)\sigma_{\rm tot}\rho}, \tag{3}$$

where $a = m_D/2T$, with m_D being the screening mass regulating the angular dependence of the cross section, while $g(a)$ is the proper function accounting for the pertinent relaxation time $\tau_\eta^{-1} = g(a)\sigma_{\rm tot}\rho$ associated to the shear transport coefficient and it is given by:

$$g(a) = \frac{1}{50}\int dy y^6 \left[\left(y^2+\frac{1}{3}\right)K_3(2y) - yK_2(2y)\right] h\left(\frac{a^2}{y^2}\right), \quad (4)$$

where K_n's are the Bessel functions and the function h relate the transport cross section to the total cross section $\sigma_{\rm tr}(s) = \sigma_{\rm tot}\, h(m_D^2/s)$ with $h(\zeta) = 4\zeta(1+\zeta)[(2\zeta+1)\ln(1+1/\zeta) - 2]$.

In order to study the role of the η/s ratio and its temperature dependence we consider three different cases: one with a constant $4\pi\eta/s = 1$ during all the evolution of the system dashed line in Fig. 1, another one with $4\pi\eta/s = 1$ at higher temperature in the QGP phase and an increasing η/s in the crossover region towards the estimated value for hadronic matter $4\pi\eta/s \approx 6$ [25,40] shown by solid line in Fig. 1. Such an increase of η/s in the crossover region $0.8T_C \leqslant T \leqslant 1.2T_C$ allows for a smooth realistic realization of the kinetic freeze out. This is because at lower temperature, according to the formula Eq. (3) $\sigma \propto (\eta/s)^{-1}$, i.e., the increase of η/s towards the estimated value for the hadronic matter, implies the total cross section decreases and this permits us to achieve in a self-consistent way the kinetic freeze out. In the following discussion the term "f.o." means to take into account the increase of η/s at low temperature. The third one is shown in Fig. 1 by the dot-dashed line. In this case we consider the increase of η/s at higher temperature with a linear temperature dependence and a minimum close to the critical temperature with a temperature dependence similar to that expected from general considerations as shown in Fig. 1.

III. INITIAL CONDITIONS

The main feature in the present paper is the implementation of initial-state fluctuations in a transport cascade approach. We will consider two systems at different centralities: Au + Au collisions at $\sqrt{s_{NN}} = 200$ GeV produced at RHIC and Pb + Pb collisions at $\sqrt{s_{NN}} = 2.76$ TeV at LHC. In particular in this section we discuss the implementation of the initial-state fluctuations in the above transport approach. In order to generate an event-by-event initial profile we use the Monte Carlo Glauber model. In this model the Woods-Saxon distribution is used to sample randomly the positions of the nucleons in the two colliding nuclei A and B. In this way a discrete distribution for these nucleons is generated. We employ the geometrical method to determine if the two nucleons one from the nucleus A and the other one from the nucleus B are colliding. Within this method two nucleons collide with each other if the relative distance in the transverse plane is $d_T \leqslant \sqrt{\sigma_{NN}/\pi}$ where σ_{NN} is the nucleon-nucleon cross section. In our calculations we have used $\sigma_{NN} = 4.2$ fm^2 for RHIC and $\sigma_{NN} = 7.0$ fm^2 for LHC. $N_{\rm coll}$ and $N_{\rm part}$ are given by counting the number of collisions and the number of participating nucleons for each event. The next step is the conversion of the discrete distribution for the nucleons into a smooth one by assuming for each nucleon a Gaussian distribution centered in the nucleon position. In our model we choose to convert the information of the nucleon distribution into the density in the transverse plane $\rho_T(x,y)$, which is given by the following sum

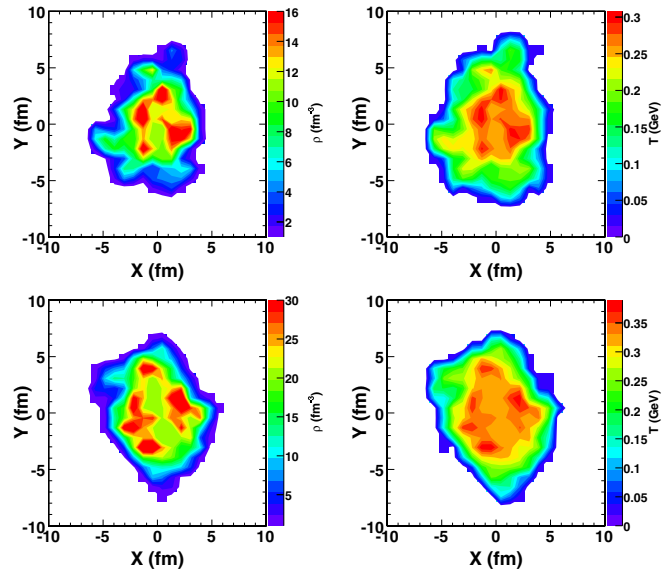

FIG. 2. (Color online) In the left column it is shown the initial transverse density $\rho_T(x,y)$ at midrapidity for two typical events for Au + Au at $\sqrt{s_{NN}} = 200$ GeV (top) and Pb + Pb at $\sqrt{s_{NN}} = 2.76$ TeV (bottom). In the right column is shown the corresponding initial temperature in transverse plane. These plots are for an impact parameter of $b = 7.5$ fm.

$$\rho_T(x,y) = C\sum_{i=1}^{N_{\rm part}} \exp\left[-\frac{(x-x_i)^2+(y-y_i)^2}{2\sigma_{xy}^2}\right], \quad (5)$$

where C is an overall normalization factor fixed by the longitudinal distribution dN/dy while σ_{xy} is the Gaussian width, which regulates the smearing of the fluctuations and in the following calculations it has been fixed to $\sigma_{xy} = 0.5$ fm. In our calculation we have assumed initially a longitudinal boost invariant distribution from $y = -2.5$ to $y = 2.5$. In the first column of Fig. 2 it is shown the contour plot of the initial transverse density at midrapidity for a given event with impact parameter $b = 7.5$ fm. The top panel refers to the system Au + Au at $\sqrt{s_{NN}} = 200$ GeV and the bottom panel to Pb + Pb at $\sqrt{s_{NN}} = 2.76$ TeV.

The transverse density $\rho_T(x,y)$ fixes the initial anisotropy in coordinate space that is quantified in terms of the following coefficients ϵ_n:

$$\epsilon_n = \frac{\sqrt{\langle r_T^n \cos(n\phi)\rangle^2 + \langle r_T^n \sin(n\phi)\rangle^2}}{\langle r_T^n\rangle}, \quad (6)$$

where $r_T = \sqrt{x^2+y^2}$ and $\phi = \arctan(y/x)$ is the polar coordinate in the transverse plane. In Fig. 3 it is shown the initial spatial anisotropies ϵ_2, ϵ_3, ϵ_4, and ϵ_5 as a function of the impact parameter. The second coefficient ϵ_2 shows a stronger dependence with the impact parameter with respect to the other coefficients because it acquires a contribution due to the global almond shape of the fireball while the other harmonics have

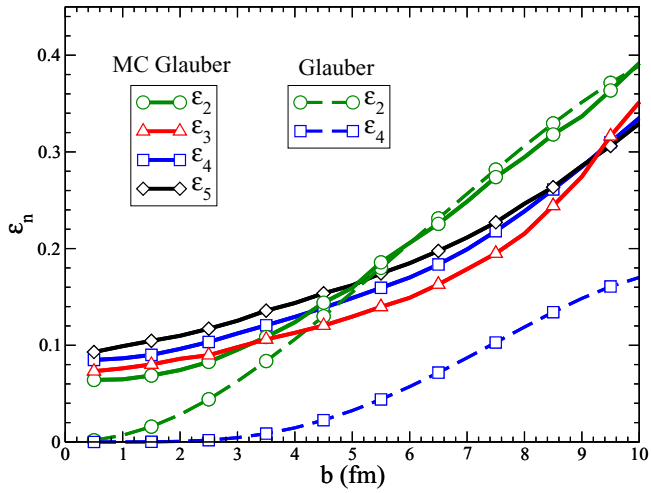

FIG. 3. (Color online) Initial spacial anisotropies ϵ_n as a function of the impact parameter. Different symbols are for different n. The solid lines refer to the Monte Carlo Glauber while the dashed ones to the optical Glauber model.

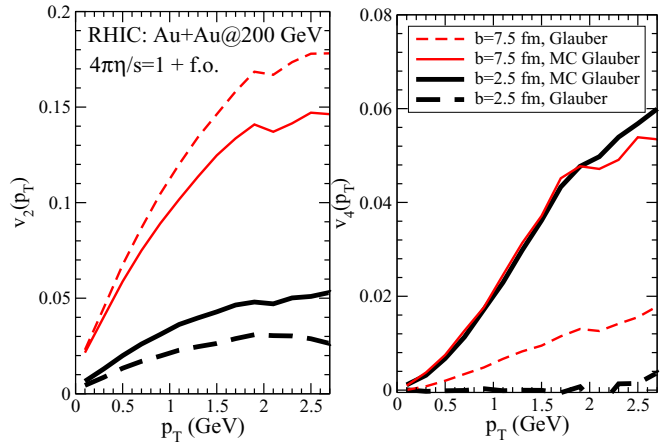

FIG. 4. (Color online) Results for Au + Au collisions at $\sqrt{s_{NN}} = 200$ GeV for mid rapidity. Left: differential elliptic flow $v_2(p_T)$ at mid rapidity. The solid lines refer to the case with initial-state fluctuations the dashed lines are for the case without initial fluctuations. Thick lines are for $b = 2.5$ fm while thin lines for $b = 7.5$ fm. Right: differential $v_4(p_T)$ at mid rapidity with the same legend as in the left panel.

most of their origin in the fluctuations of the positions of the nucleons. For more central collisions $b \leqslant 2.5$ fm the ϵ_2 is even smaller than the other harmonics because when the effect of the elliptic overlap region disappears it becomes more difficult to have fluctuations of the positions of the nucleons along only one preferential direction.

For the initialization in momentum space at RHIC (LHC) energies we have considered for partons with transverse momentum $p_T \leqslant p_0 = 2$ GeV (3 GeV) a thermalized spectrum in the transverse plane. Assuming the local equilibrium the initial local temperature in the transverse plane $T(x,y)$ is evaluated by using the standard thermodynamical relation $\rho_T(x,y) = \gamma T^3/\pi^2$ with $\gamma = 2 \times (N_c^2 - 1) + 2 \times 2 \times N_c \times N_f = 40$ with $N_c = 3$ and $N_f = 2$. In the right column of Fig. 2 it is shown the corresponding initial local temperature in transverse plane. As shown in the central region of the fireball for midperipheral collision we can reach temperature $T \approx 300$ MeV at RHIC and $T \approx 400$ MeV at LHC. While for partons with $p_T > p_0$ we have assumed the spectrum of nonquenched minijets according to standard NLO-pQCD calculations with a power-law shape [41,42]. In coordinate space the partons with $p_T > p_0$ have been distributed according the binary collisions. The initial transverse momentum of the particles is distributed uniformly in the azimuthal angle. We fix the initial time of the simulation to $\tau_0 = 0.6\,\text{fm}/c$ for RHIC and $\tau_0 = 0.3\,\text{fm}/c$ for LHC.

In the following discussion, we will consider two different types of initial conditions. One consisting in a fixed initial distribution by using the standard Glauber model as used in previous works, see Refs. [5,7,22,30]. The second one consisting of an initial profile changing event by event according to the MC Glauber model as discussed before.

In our simulations we have used $N_{\text{event}} = 500$ events for each centrality class. This number is enough to get solid results for the spectra, differential elliptic flow, and high order flow coefficients $v_n(p_t)$. For the study of the correlations between the initial ϵ_n and the final v_n that will be shown in the next section we have extended this analysis to 10^3 events. The inclusion of the initial-state fluctuations introduces further difficulties because in order to get stable results we need to have a good sampling of the initial geometry event by event and this is controlled by the total number of test particles N_{test}. Furthermore, an irregular initial profile need a good calculation grid resolution. We have checked the convergency of our results for v_2, v_3, and v_4 with the lattice spacing of the calculation grid and N_{test}. We found the convergency for a grid with a transverse area of the cell $A_T = 0.12\,\text{fm}^2$ and $N_{\text{test}} = 2\times10^6$ as the total number of test particles per event.

The elliptic flow $v_2(p_T)$ and the high order harmonics $v_3(p_t)$, $v_4(p_T)$, and $v_5(p_T)$ have been calculated as

$$v_n = \langle \cos\left[n(\phi - \Psi_n)\right] \rangle, \tag{7}$$

where the momentum space angles Ψ_n are given by

$$\Psi_n = \frac{1}{n} \arctan \frac{\langle \sin(n\phi) \rangle}{\langle \cos(n\phi) \rangle}. \tag{8}$$

In this section first we discuss the comparison between the Glauber model without initial fluctuations with the MC Glauber with fluctuations. Without initial-state fluctuations only even harmonics can be generated therefore we will consider here only $v_2(p_T)$ and $v_4(p_T)$. In the left panel of Fig. 4 we compare the differential elliptic flow $v_2(p_T)$ obtained with an initial state that changes event by event according to the MC Glauber model (solid lines) as discussed in detail the previous section with the one obtained for the case with an averaged initial profile (dashed lines). These results are for Au + Au collisions at $\sqrt{s} = 200$ GeV and for 20–30% centrality class. In these calculations we have considered $4\pi\eta/s = 1$ at high temperature and an increasing η/s at lower temperature as shown by the red solid line in Fig. 1. As shown for midperipheral collision (with $b = 7.5$ fm) the effect of the fluctuations in the initial geometry is to reduce the $v_2(p_T)$ of

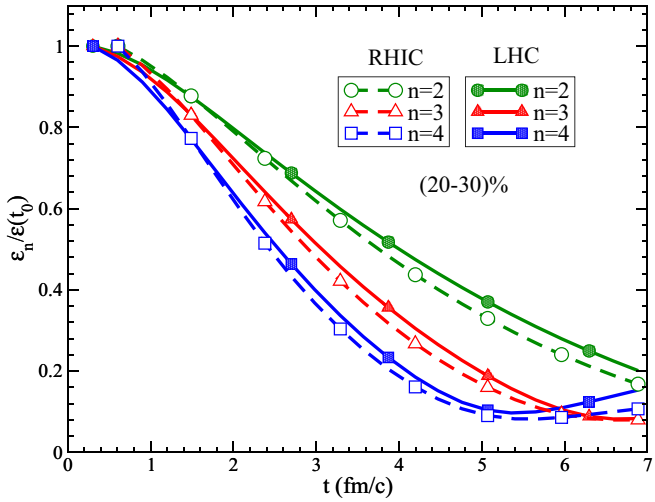

FIG. 5. (Color online) $\epsilon_n/\epsilon_n(t_0)$ as a function of the time for Au + Au collisions at $\sqrt{s_{NN}} = 200$ GeV (dashed lines) and for Pb + Pb collisions at $\sqrt{s_{NN}} = 2.76$ TeV (solid lines). Different symbols refer to different harmonics n.

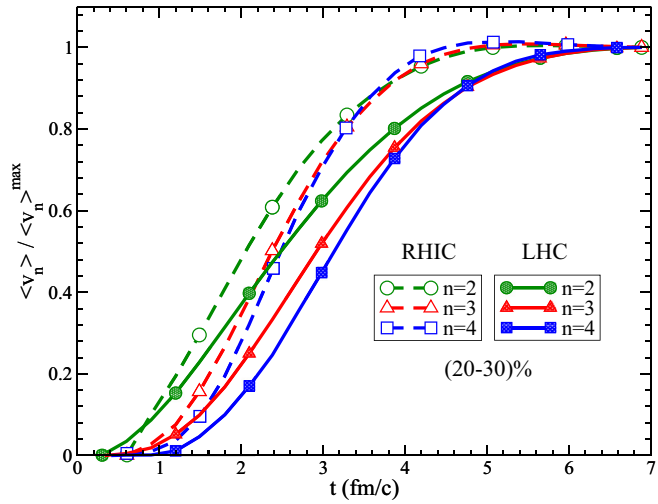

FIG. 6. (Color online) $\langle v_n \rangle / \langle v_n \rangle^{\max}$ as a function of time at midrapidity and for (20–30)% of centrality. Dashed lines are the results for Au + Au at $\sqrt{s_{NN}} = 200$ GeV while solid lines Pb + Pb at $\sqrt{s_{NN}} = 2.76$ TeV. Different symbols correspond to different harmonics.

about 15%, despite the same initial eccentricity ϵ_2 in Glauber and Monte Carlo Glauber, see green solid and dashed lines in Fig. 3. The reduced efficiency in building up the $v_2(p_T)$ is related to the fact that for an irregular geometry in the transverse plane the pressure gradients generate also a small counterflow towards the inner part of the fireball reducing the azimuthal anisotropy in momentum space due to the global almond shape. The introduction of the fluctuations in the initial geometry play the role to generate the higher-order harmonics in particular the odd harmonics, which were absent by symmetry in the averaged initial configuration. In the right panel of Fig. 4 we show the same comparison for the quadrangular flow $v_4(p_T)$. We observe an opposite behavior: the initial-state fluctuations increase the final $v_4(p_T)$ by a factor of 3. This result is related to the fact that the fluctuations introduce about a factor 3 larger initial ϵ_4 as shown by the comparison between blue solid and dashed lines in Fig. 3. In other words for midperipheral collisions most of $v_2(p_T)$ comes from the global almond shape while $v_4(p_T)$ comes normally from the initial fluctuations. In fact, as shown by the black thick solid and dashed lines in the left panel of Fig. 3 the effect of the fluctuations is to produce a larger $v_2(p_T)$. From the comparison between thick black solid and dashed line in the right panel of Fig. 3 we observe a nonzero $v_4(p_T)$ that was absent in the averaged initial profile where the initial $\epsilon_4 \approx 0$ (see blue dashed line in Fig. 3). Moreover we observe a low sensitivity of $v_4(p_T)$ with the centrality similarly to the experimental data at RHIC energies [10]. Such a behavior would be impossible to explain without initial-state fluctuations.

IV. EFFECTS OF $\eta/s(T)$ ON THE $v_n(p_T)$

In the first part of this section we discuss the time evolution of the eccentricities ϵ_n and the anisotropic flows coefficients $\langle v_n \rangle$ for Au + Au collisions at $\sqrt{s} = 200$ GeV (solid lines) and for Pb + Pb collisions at $\sqrt{s} = 2.76$ TeV. In Fig. 5 we plot the time evolution of the ϵ_n normalized to the initial eccentricity $\epsilon_n(t_0 = 0.6\,\mathrm{fm}/c)$ for RHIC and $\epsilon_n(t_0 = 0.3\,\mathrm{fm}/c)$ for LHC. At very early times the small deformation of the fireball in the transverse plane decrease linearly with time and at first order of this deformation we have that $\epsilon_n \propto \epsilon_n(t_0) - \alpha_n\, t^{n-2}$. This gives the ordering in the time evolution of ϵ_n shown in Fig. 5. the time evolution of ϵ_n is faster for larger n.

On contrary v_n show an opposite behavior during the early times of the expansion of the fireball. In Fig. 6 it shown the average $\langle v_n \rangle$ normalized to its maximum value at the end of the expansion. The $\langle v_n \rangle$ appear later for larger n and their development is flatter at early times for larger n. Similar results have been obtained in a 2 + 1D transport approach where considerations on the early times evolution of the fireball give that $\langle v_n \rangle \propto t^n$ [43,44]. As shown in left panel of Fig. 7 we observe that in the time evolution of the different harmonics $\langle v_n \rangle$ the ordering is present also at late times. In right panel of Fig. 7 it is shown the production rate for the different harmonics and as shown different harmonics have different production rates. In particular, we observe that at very early time the second harmonic has a nonzero value for $\frac{d\langle v_2 \rangle}{dt} \neq 0$ at variance with higher harmonics for which $\frac{d\langle v_n \rangle}{dt} \approx 0$. This different behavior could be the origin of the stronger correlation between the final elliptic flow v_2 and its initial eccentricity ϵ_2 that becomes weaker between the final v_n and the initial ϵ_n for higher harmonics ($n > 2$), see Sec. V.

Differential flow coefficients $v_n(p_T)$ are observables that carry out more information about the fireball created in the heavy ion collisions in particular because they are sensitive to the transport properties of the medium such as the η/s ratio. In the following discussion we will study the effect of the η/s on the buildup of the elliptic flow $v_2(p_T)$ and on the high order harmonics $v_3(p_T)$, $v_4(p_T)$, and $v_5(p_T)$. With $v_n(p_T)$ we mean the root mean square $\sqrt{\langle v_n^2 \rangle}$ as it has been done in experimental data using the event plane method. In the top panel of Fig. 8

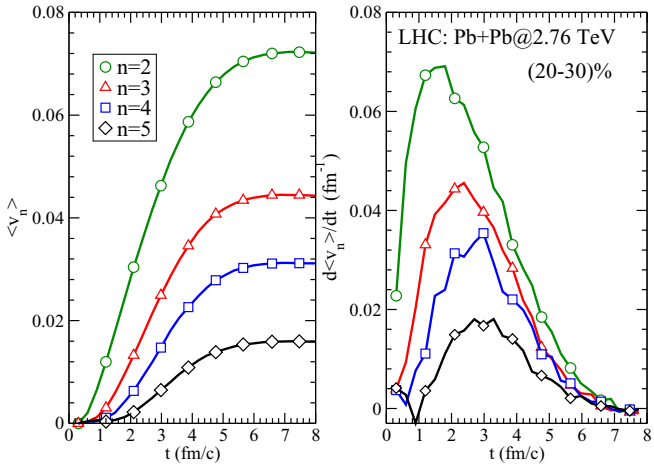

FIG. 7. (Color online) Left: Time evolution of $\langle v_n \rangle$ at midrapidity respectively for (20–30)% centrality collisions. Different symbols are for different harmonics. Right: Production rate $\frac{d\langle v_n \rangle}{dt}$ as a function of time at midrapidity and for the same centrality. These results are for Pb + Pb collision at $\sqrt{s_{NN}} = 2.76$ TeV.

it is shown the elliptic flow $v_2(p_T)$ (green thick lines) and the $v_4(p_T)$ (blue thin lines) at midrapidity and for (20–30)% centrality for both RHIC Au + Au at $\sqrt{s} = 200$ GeV (left panel) and LHC Pb + Pb at $\sqrt{s} = 2.76$ TeV (right panel). In general in agreement with what has been obtained in viscous hydrodynamical calculations, the increase of the viscosity of the medium has the effect to reduce both v_2 and v_4.

As we can see at RHIC energies comparing the thick dashed lines with the solid ones, in the left panel of Fig. 8, the $v_2(p_T)$ is sensitive to the increase of the η/s at lower temperature close to the crossover region. In particular the effect is a reduction of the elliptic flow of about 17%. A similar trend was observed for the fourth harmonic $v_4(p_T)$ where we have a reduction due to the increase of η/s at lower temperature but the effect in this case is about a factor of two larger than the previous one, i.e., about 30–40%. The different sensitivity to the η/s can be attributed to their different formation time, $t_{v_4} > t_{v_2}$ [38]. As shown in Fig. 6 each harmonics v_n starts to develop at different times. In particular v_4 has its maximum development approximatively at $\tau \approx 3\,\mathrm{fm}/c$ while the v_2 at $\tau \approx 1.2\,\mathrm{fm}/c$. This means that different harmonics probe mainly different temperatures and different value of the η/s ratio. Assuming that the first few fm/c of the expanding fireball are dominated by the one-dimensional (1D) longitudinal expansion [32] where approximatively $T(\tau) = T_0(\tau_0/\tau)^{1/3}$ we have that when v_4 has its maximum development at about $\tau \approx 3\,\mathrm{fm}/c$ the temperature is $1.3\,T_C$ at RHIC and $2\,T_C$ at LHC. In other words, this tells us that v_4 at RHIC energies mainly develops closer to the crossover region where η/s should increase.

On the other hand, at LHC energies, left panel of Fig. 8, the scenario is different, the elliptic flow is almost unaffected by the increase of η/s ratio at low temperature (in the hadronic phase) as we can see comparing the green thick dashed line with the solid one. Instead we observe that the increase of η/s at lower temperature has a more sensitive effect on the $v_4(p_T)$ with a reduction of about 5–10%, see blue solid and

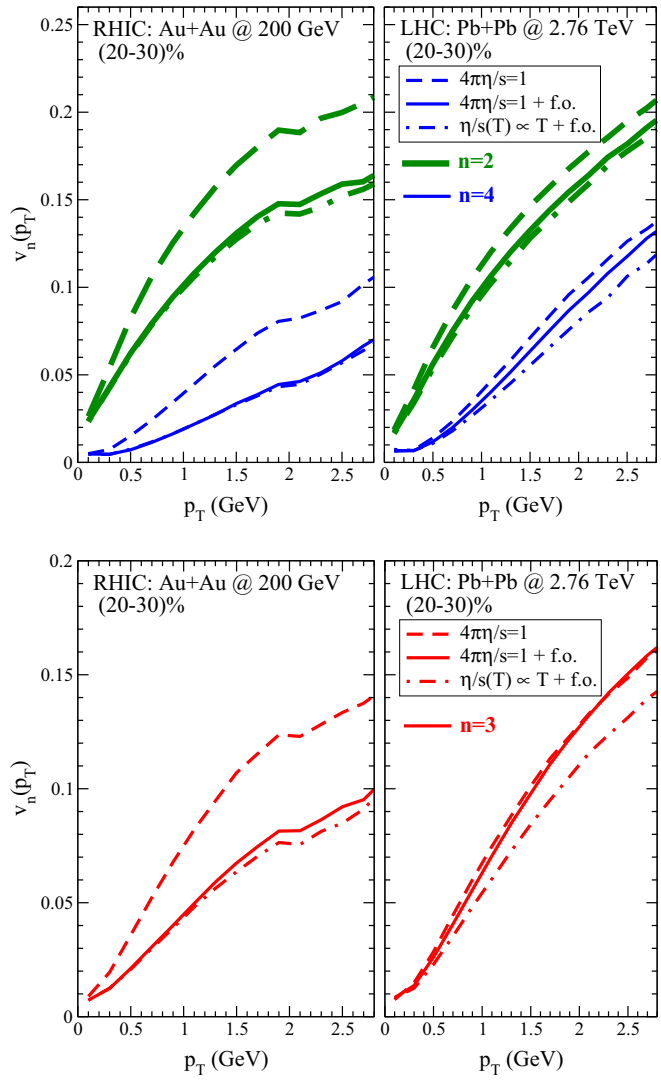

FIG. 8. (Color online) Top: Differential $v_2(p_T)$ (thick lines) and $v_4(p_T)$ (thin lines) green and blue lines respectively at midrapidity and for (20–30)% collision centrality. The comparison is between the two systems: Au + Au at $\sqrt{s} = 200$ GeV (left) and Pb + Pb at $\sqrt{s} = 2.76$ TeV (right). The dashed lines refer to the case with a constant $\eta/s = (4\pi)^{-1}$ during all the evolution. The solid lines refer to the case with $\eta/s = (4\pi)^{-1}$ at higher temperature and with an increasing η/s ratio at lower temperature while the dot dashed lines refer to the case with $\eta/s \propto T$ at higher temperature and with an increasing η/s ratio at lower temperature. Right: Differential $v_3(p_T)$ in red lines with the same legend as in the top panel.

dashed lines. Again this different sensitivity to the η/s in the crossover region between v_2 and v_4 at LHC is consistent with the results obtained at RHIC energies and depends on the different formation time of the harmonics in relation to the initial T of the system. The greater sensitivity at RHIC energies of both v_2 and v_4 to the η/s at low temperature is related to the different lifetime of the fireball. In fact the lifetime of the fireball at LHC is greater than that at RHIC, 8–10 fm/c at LHC against 4–5 fm/c at RHIC. In general this means that at RHIC energies the v_n have not enough time to fully

develop in the QGP phase. While at LHC energies we have that the v_n develops almost completely in the QGP phase and therefore it is less sensitive to the dynamics in the crossover and hadronic region. This result were first found without initial-state fluctuation in Refs. [7,30,45] but remains similar also with fluctuations. The last, however, allows us to study for the first time a similar effect also on $v_3(p_T)$.

In Fig. 8 is shown the effect of an $\eta/s(T)$ in the QGP phase. In the comparison between the solid lines and the dot dashed ones the only difference is in the linear temperature dependence of $\eta/s \propto T$ for $T > T_C$ while at lower temperature we have the same dependence (see dot dashed lines in Fig. 1). As we can see the v_4 at LHC is sensitive to the change of η/s at higher temperature while at RHIC energies the v_4 is completely unaffected by this change. In the bottom panel of Fig. 8 it is shown the triangular flow $v_3(p_T)$ (red lines) at midrapidity for (20–30)% centrality and for both RHIC Au + Au at $\sqrt{s} = 200$ GeV (left panel) and LHC Pb + Pb at $\sqrt{s} = 2.76$ TeV (right panel). In agreement with what has been obtained for the even harmonics v_2 and v_4, we observe at RHIC energies a reduction of $v_3(p_T)$ due to the increase of the η/s at low temperature with a reduction of about 25%, while at LHC it is almost insensitive to the change of η/s in the crossover region. However we observe that at LHC the third and fourth harmonics are more sensitive to the change of $\eta/s(T)$ with respect to the elliptic flow with a deviation of about 10% for v_3 and v_4 against a less 5% for v_2. Still it has be noted that such a sensitivity is quite small to hoping a determination of the T dependence of η/s from the $v_n(p_T)$.

Very recently it has been possible to access also experimentally to the ultracentral collisions. The ultracentral collisions are interesting because the initial ϵ_n come completely from the fluctuations in the initial geometry rather than by global geometric overlap region. In Fig. 9 is shown the comparison of

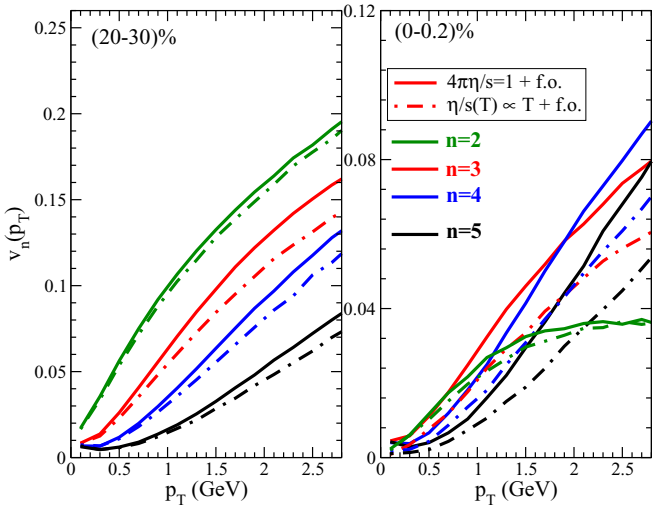

FIG. 9. (Color online) Comparison between $v_n(p_T)$ for midperipheral (left) and central (right) collision. Different colors refer to different harmonics while solid lines correspond to $4\pi\eta/s = 1$ in QGP phase and f.o. and dot dashed lines to $\eta/s \propto T$ in the QGP phase and f.o.

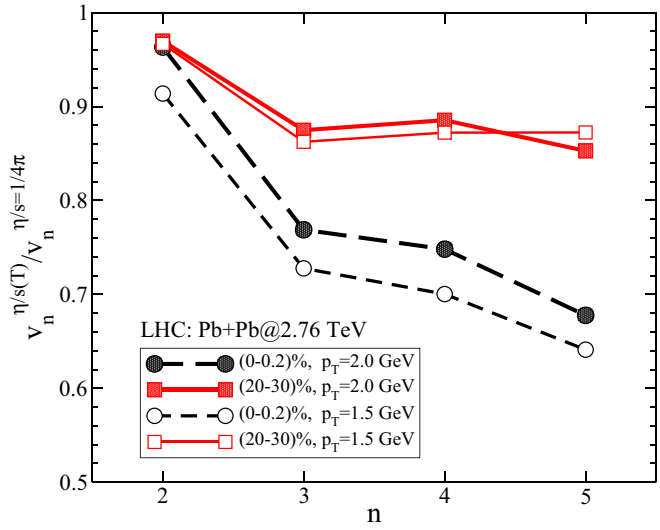

FIG. 10. (Color online) Ratio between $v_n(p_T)$ for two different parametrizations of η/s as a function of the order of the harmonic n and for $p_T = 1.5$ GeV (open symbols) and $p_T = 2$ GeV (full symbols). Solid lines refer to midperipheral collisions while dashed lines to ultracentral collisions.

$v_n(p_T)$ produced in Pb + Pb at $\sqrt{s} = 2.76$ TeV collisions for different centralities: left panel for midperipheral collisions and right panel for central collisions. Different colors are for different harmonics. Solid lines refer to the case with $\eta/s = 1/(4\pi)$ in the QGP phase and the increase at low temperature as shown in Fig. 1 by red solid lines while the dot-dashed lines refer to the case with $\eta/s \propto T$ in the QGP phase and the increase at low temperature as shown in Fig. 1 by blue dot dashed lines. From the comparison we observe that at low p_T both centralities the $v_n(p_T)$ are much flatter for larger n. This results is in agreement with that obtained in hydrodynamic calculations where $v_n(p_T) \propto p_T^n$ [46]. On the other hand at high p_T for ultracentral collisions we observe that the elliptic flow $v_2(p_T)$ shows a saturation while for $n \geqslant 3 v_n(p_T)$ increase linearly with p_T. This is in qualitative agreement with what has been observed experimentally, but a quantitative comparison would require the inclusion of hadronization, which, however, would not affect the sensitivity to $\eta/s(T)$. In particular the sensitivity to the value of η/s in the QGP phase increase with the increasing the order of the harmonics n in agreement with the fact that viscous corrections to $v_n(p_T)$ increase with the harmonics [35]. Furthermore we observe that reduction of $v_n(p_T)$ due to the increase of η/s in the QGP phase (dot dashed lines) is strongly enhanced for ultracentral collisions. As shown in Fig. 10 for $n \geqslant 3$ the reduction for central collisions is about 30–35% against a reduction of about 10% for midperipheral collisions. It is indeed remarkable that a 30% effect is determined by a slowly linear rising of η/s with T as the one considered and depicted in Fig. 1. In particular, in central collisions higher harmonics acquire a larger sensitivity to the value of the viscosity in the QGP phase. Therefore our study suggests that to have information about $\eta/s(T)$ one should focus on ultracentral collisions. This point is further strengthened by the study of

the correlations between v_n and the initial eccentricities ϵ_n, which we discuss in the next section.

V. CORRELATIONS BETWEEN v_n AND ϵ_n

In recent years, the correlation between integrated v_2 and high order harmonics v_3, v_4 with the initial asymmetry in coordinate space ϵ_2,ϵ_3, and ϵ_4 have been studied in the event-by-event ideal and viscous hydrodynamics framework [47–49]. In general it has been shown that the elliptic flow is strongly correlated with initial eccentricity while a weaker correlation has been found for higher harmonics v_3,v_4, with ϵ_3 and ϵ_4. One explanation for the weak correlation observed between v_4 and ϵ_4 is that for final v_4 there is also a correlation with the initial ϵ_2. In particular, in Ref. [47] it has been shown that it possible to have a good linear correlation between v_4 and a linear combination of the initial ϵ_2 and ϵ_4.

In this section we discuss these correlations within an event-by-event transport approach with initial-state fluctuations. A measure of the linear correlation is given by the correlation coefficient $C(n,m)$ given by the following expression:

$$C(n,m) = \frac{\sum_i \left(\epsilon_n^i - \langle\epsilon_n\rangle\right)\left(v_m^i - \langle v_m\rangle\right)}{\sqrt{\sum_i \left(\epsilon_n^i - \langle\epsilon_n\rangle\right)^2 \sum_i \left(v_m^i - \langle v_m\rangle\right)^2}}, \quad (9)$$

where ϵ_n^i and v_m^i are the values of ϵ_n and v_m corresponding to the given event i and evaluated according Eqs. (6) and (7). $C(n,m) \approx 1$ corresponds to a strong linear correlation between the initial ϵ_n and the final v_m.

The results shown in this section have been obtained with $N_{\text{event}} = 1000$ events for each centrality class and a total number of test particles per event of $N_{\text{test}} = 2\times10^6$. In Fig. 11, it is shown the two-dimensional plots of the integrated flow coefficients v_n as a function of the corresponding initial ϵ_n for each event. The results shown are for Au + Au collisions at $\sqrt{s_{NN}} = 200$ GeV and for three different centralities (10–20)%, (20–30)%, and (30–40)%. The viscosity has been fixed to $4\pi\eta/s = 1$ plus a kinetic f.o. realized by the increase in $\eta/s(T)$ as in Fig. 1. As shown in the top panel we observe a stronger linear correlation

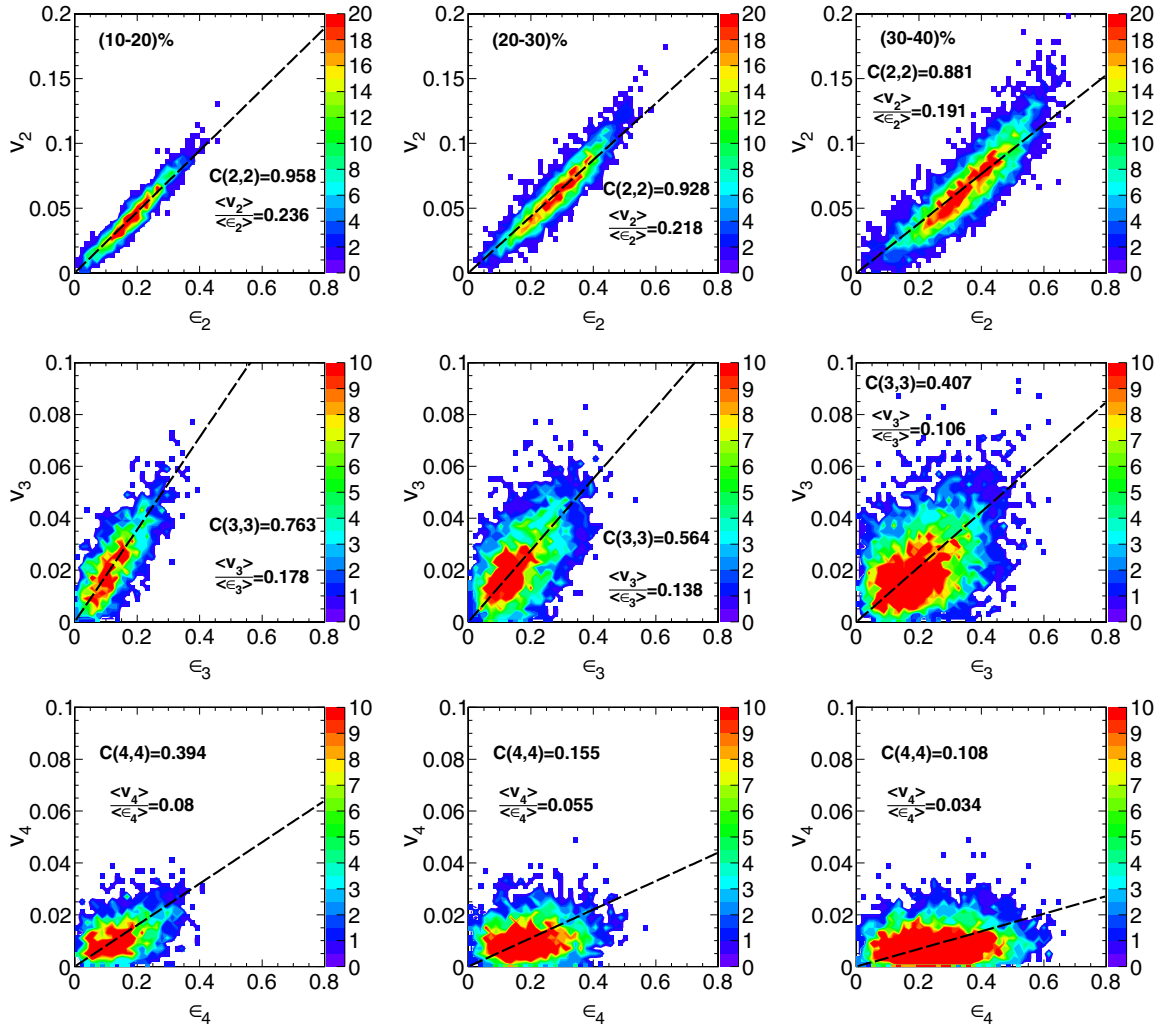

FIG. 11. (Color online) ϵ_n and v_n for Au + Au collisions at $\sqrt{s_{NN}} = 200$ GeV and for three different centrality class. Top: ϵ_2 and v_2 for (10–20)%, (20–30)%, and (30–40)% from left to right. Middle: ϵ_3 and v_3 for the same centralities. Finally in the bottom panel ϵ_4 and v_4. In these calculations we have fixed $\eta/s = 1/(4\pi)$ for high temperature and the kinetic f.o. at lower temperature (see solid line in Fig. 1).

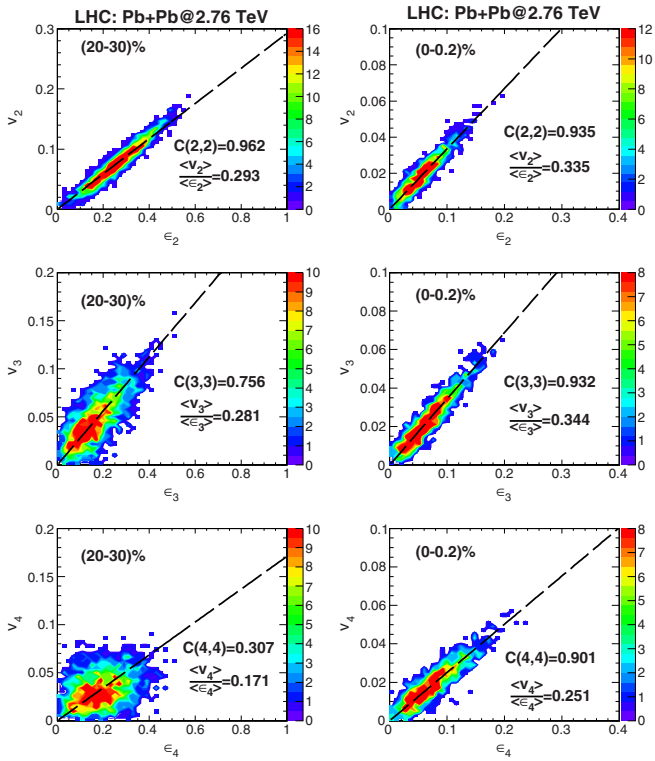

FIG. 12. (Color online) ϵ_n and v_n for Pb + Pb collisions at $\sqrt{s_{NN}} = 2.76$ TeV and for (20–30)% and (0–0.2)% centrality cut, respectively right and left panel. In these calculations we have fixed $\eta/s = 1/(4\pi)$ for high temperature and the kinetic f.o. at lower temperature (see solid line in Fig. 1).

between ϵ_2 and v_2 for midcentral collisions with a linear correlation coefficient that shows a monotonic behaviour with the collision centrality from $C(2,2) \approx 0.96$ for (10–20)% to $C(2,2) \approx 0.89$ for (30–40)%. Qualitatively the results are in agreement with the one obtained within a 2+1D viscous hydrodynamics, see Ref. [49]. In general we observe a slightly smaller degree of correlation probably induced by the fact that we simulate a 3+1D expansion that can be expected to contribute to the decorrelation. In the middle and bottom panel of Fig. 11 we have shown similar plots for the third and fourth harmonics. We observe again a reduction of the correlation coefficient with the centrality of the collision similarly to v_2 and ϵ_2. We obtain that the correlation between ϵ_3 and v_3 for all the collision centralities is weaker with respect to that obtained for the elliptic flow. Furthermore the fourth harmonic flow v_4 shows a weak correlation with the initial ϵ_4 in particular for midperipheral collisions where the linear correlation coefficient is quite weak $C(4,4) < 0.3$. Furthermore we observe that the $\langle v_n \rangle/\epsilon_n$ ratio (see dashed lines in Fig. 11) decreases when the correlation coefficient $C(n,n)$ decreases, i.e., for more peripheral collisions.

A similar behavior for the linear correlation coefficient $C(n,n)$ is observed at LHC energies for Pb + Pb collisions at $\sqrt{s_{NN}} = 2.76$ TeV. In Fig. 12 is shown the comparison between ultracentral and midperipheral collision at LHC energies at $\sqrt{s_{NN}} = 2.76$ TeV. In ultracentral collisions the $\langle v_n \rangle$ are more correlated to the initial ϵ_n than at peripheral

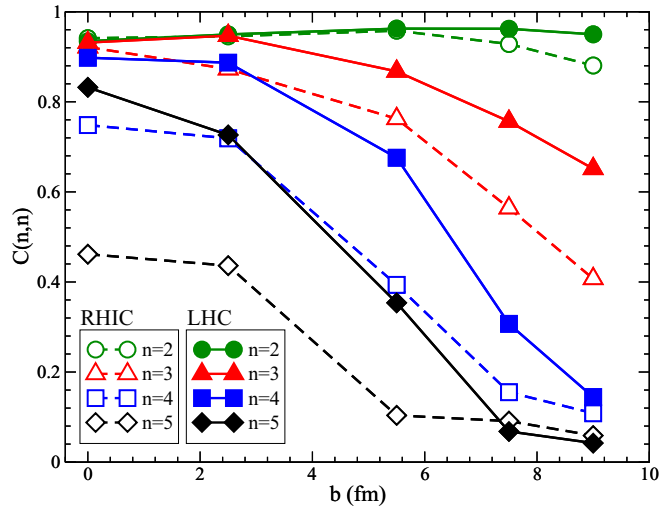

FIG. 13. (Color online) Correlation coefficient $C(n,n)$ as a function of the impact parameter b. Different symbols refer to different harmonics n. In particular circles, triangles, squares and diamonds refer to $n = 2,3,4$, and 5 respectively. The solid lines correspond to Au + Au collisions at $\sqrt{s_{NN}} = 200$ GeV while dashed lines to the system Pb + Pb at $\sqrt{s_{NN}} = 2.76$ TeV.

collisions and very interesting differences emerge looking also at higher harmonics.

In order to better visualize and discuss such differences we have plot in Fig. 13 the $C(n,n)$ as a function of the impact parameter for both RHIC (dashed lines) and LHC energies (solid lines). As shown the linear correlation coefficient is a decreasing function of the impact parameter for all the harmonics. However, as we can see comparing the dashed and solid lines show, at LHC energies there is a stronger correlation between ϵ_n and v_n for all n with respect to RHIC energies. We observe that v_2 and ϵ_2 have the same degree of correlation for both RHIC and LHC energies while a lower degree of correlation it is shown for higher harmonics $n = 3, 4$, and $n = 5$. More interesting is the fact that for ultracentral collisions at LHC the linear correlation coefficient $C(n,n)$ remains above 0.9 for $n = 2,3,4$ and even the $n = 5$ shows large $C(n,n) = 0.85$. This can be visualized also in the right panel of Fig. 12 where the (v_n,ϵ_n) correlation plot is shown in midperipheral (20–30%) collisions (left panel) and in ultracentral collisions (0–0.2%) (right panels).

The strong correlation observed for ultracentral collisions means that the value obtained for $\langle v_n \rangle$ and its dependence with the harmonics n for those collisions is strongly related to the value of the initial asymmetry measure ϵ_n. In particular this could imply that the structure of the $v_n(p_T)$ at LHC where $C(n,n) \approx 1$ carry out information about the initial geometry of the fluctuations. This joined to the observation that for ultracentral collisions the sensitivity of v_n to η/s is increased by about a factor of 2–3 strongly suggests to focus the experimental efforts at LHC highest energy and ultracentral collisions.

To study the effect of the viscosity and its possible temperature dependence on the correlation we have studied how change the correlation coefficient with the different parametrizations for η/s. In Table I we show the results for

TABLE I. Linear correlation coefficient $C(n,n)$ for RHIC and LHC energies and for different temperature parametrization of η/s. These results are for (20–30)% centrality class.

$C(n,n)$	n	$4\pi\eta/s = 1$	$4\pi\eta/s = 1 + \text{f.o.}$	$\eta/s \propto T + \text{f.o.}$
	2	0.95	0.94	0.93
RHIC	3	0.70	0.58	0.65
	4	0.30	0.28	0.31
	2	0.96	0.96	0.96
LHC	3	0.78	0.78	0.74
	4	0.39	0.38	0.38

$C(n,n)$ for the two energies RHIC and LHC for (20–30)% centrality class. In general for this centrality we observe that at LHC energies and for all the viscosities considered the degree of correlation between ϵ_n and v_n is greater than the one at RHIC energies. Moreover, we obtain that at LHC the correlation coefficient is not sensitive to the change of the viscosity both at low and high temperature. A slight different behavior we have at RHIC energies where the effect of the kinetic freeze out is to reduce the degree of correlation between the initial ϵ_n and the final v_n. Furthermore, we have computed the nondiagonal components for the linear correlation coefficient $C(n,m)$. We found that $C(2,3) \approx 0$. and $C(3,4) \approx 0$ for all the range of centralities explored which means that there is no linear correlation between v_2 and ϵ_3 and v_3 and ϵ_4. A different behavior we observe for $C(4,2)$, which is seen to be an increasing function with the centrality $C(4,2) \approx 0.02$ for central collision ($b = 0$ fm) and about $C(4,2) \approx 0.23$ at $b = 7.8$ fm. This means that in more peripheral collisions the fourth harmonic v_4 has some contamination of ϵ_2 and it is not driven only by ϵ_4 as already suggested in Ref. [47].

Some interesting properties of the v_n distributions can be inferred by studying the centrality dependence of the relative fluctuations $\sigma_{v_n}/\langle v_n\rangle$. In Fig. 14(a) it is shown the $\langle N_{\text{part}}\rangle$ dependence of the ratios $\sigma_{v_n}/\langle v_n\rangle$ and $\sigma_{\epsilon_n}/\langle\epsilon_n\rangle$ where σ_{v_n} and σ_{ϵ_n} are the standard deviation respectively for v_n and ϵ_n. As shown for $n = 2$ we observe a strong dependence of the relative fluctuations with the centrality of the collision with $\sigma_{v_2}/\langle v_2\rangle \approx 0.4$ for $\langle N_{\text{part}}\rangle \approx 130$. For more central collisions this ratio approaches the value expected for a 2D Gaussian distribution where $\sigma_{v_n}/\langle v_n\rangle = \sqrt{4/\pi - 1} \approx 0.523$ [50], shown by the dashed line in Fig. 14. For higher harmonic $n = 3,4$, and 5 as shown in Figs. 14(b)–14(d) the values of $\sigma_{v_n}/\langle v_n\rangle$ are approximatively the same of the ones of the initial geometry with $\sigma_{v_n}/\langle v_n\rangle \approx \sigma_{\epsilon_n}/\langle\epsilon_n\rangle$ and they are almost independent of the collision centrality and for all the centralities studied they are very close to the the value $\sqrt{4/\pi - 1}$ shown by the dashed lines. These results imply that the distributions of v_3, v_4, and v_5 for all the centrality range studied are consistent with the fluctuation-only scenario discussed in Ref. [50] and these fluctuations are related to the fluctuations of the initial geometry. On the other hand, the distribution of v_2 is close to this limit for most central collisions while for midperipheral collisions there is a contribution coming from the global average geometry.

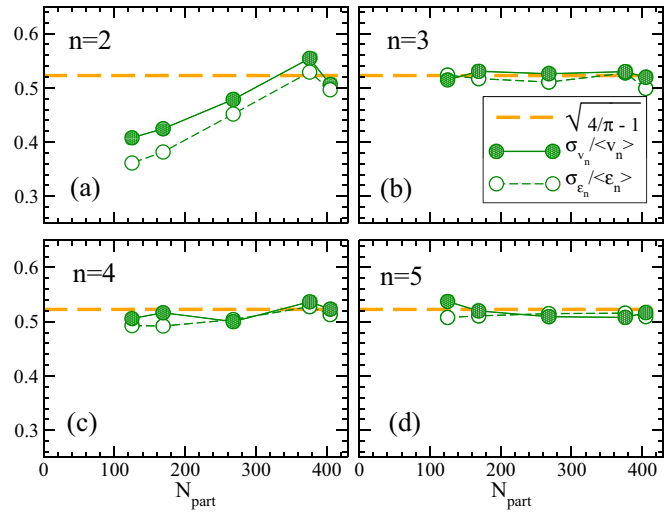

FIG. 14. (Color online) (a)–(d) $\sigma_{v_n}/\langle v_n\rangle$ (full symbols) and $\sigma_{\epsilon_n}/\langle\epsilon_n\rangle$ (open symbols) as a function of $\langle N_{\text{part}}\rangle$ respectively for $n = 2,3,4$, and 5. The dashed lines indicate the value $\sqrt{4/\pi - 1}$ expected for a 2D Gaussian distribution. These results are for Pb + Pb collisions at $\sqrt{s_{NN}} = 2.76$ TeV.

VI. CONCLUSIONS

Using an event-by-event transport approach we have investigated the buildup of the anisotropic flows $v_n(p_T)$ for $n = 2,3,4$, and 5. In particular we have studied the effect of η/s ratio on $v_n(p_T)$ for two different beam energies: at RHIC for Au + Au collisions at $\sqrt{s} = 200$ GeV and at LHC for Pb + Pb collisions at $\sqrt{s} = 2.76$ TeV. We have found that at RHIC the $v_n(p_T)$ are more affected by the value of η/s at low temperature ($T < 1.2T_C$) and the sensitivity increases with the order of the harmonics. At LHC we get a different effect, all the $v_n(p_T)$ develop in the QGP phase and are not affected by the value of η/s in the crossover region. However the sensitivity to the T dependence of the η/s is quite weak, more specifically a constant $\eta/s = 0.08$ or an $\eta/s \propto T$ induce differences in the v_2 of at most 5% and of about 10% in v_3, v_4, v_5. The novel result from our analysis is that such a scenario changes for ultracentral collisions, where we found an enhancement of the sensitivity of the $v_n(p_T)$ that for $n = 3,4,5$ reaches about 30%. We have also studied the correlation between the initial asymmetry in coordinate space, measured by ϵ_n, and the final asymmetry in momentum space given by $\langle v_n\rangle$. We have found that the larger is the collision energy, the larger is the degree of correlation between ϵ_n and $\langle v_n\rangle$. At LHC there is significantly more correlation than at RHIC. For both collision energies considered and in all the range of impact parameters studied, the v_2 is strongly correlated with the ϵ_2 with the linear correlation coefficient $C(2,2) \approx 0.95$. The degree of correlation between ϵ_n and the corresponding $\langle v_n\rangle$ decrease for higher harmonics. Moreover, in ultracentral collisions we found that $C(n,n) > 0.9$ for $n = 2,3$, and 4, which imply that the $v_n \propto \epsilon_n$ and they carry out the information about the initial geometry of the fireball. These results joined with the fact that in ultracentral collisions the $v_n(p_T)$ have a large sensitivity to the η/s ratio strongly suggest to focus the experimental effort

to those collision centralities where it is possible to get better constraint on the value of η/s in the QGP phase and gain a new insight on the initial-state fluctuations.

ACKNOWLEDGMENTS

V.G., S.P., F.S., and G.L.G. acknowledge the support of the ERC-StG Grant under the QGPDyn project.

[1] J. Adams *et al.* (STAR Collaboration), Nucl. Phys. **A757**, 102 (2005).
[2] K. Aamodt *et al.* (ALICE Collaboration), Phys. Rev. Lett. **105**, 252302 (2010).
[3] P. Romatschke and U. Romatschke, Phys. Rev. Lett. **99**, 172301 (2007).
[4] H. Song and U. W. Heinz, Phys. Rev. C **78**, 024902 (2008).
[5] G. Ferini, M. Colonna, M. Di Toro, and V. Greco, Phys. Lett. B **670**, 325 (2009).
[6] Z. Xu and C. Greiner, Phys. Rev. C **79**, 014904 (2009).
[7] S. Plumari and V. Greco, AIP Conf. Proc. **1422**, 56 (2012).
[8] P. K. Kovtun, D. T. Son, and A. O. Starinets, Phys. Rev. Lett. **94**, 111601 (2005).
[9] A. Adare *et al.* (PHENIX Collaboration), Phys. Rev. Lett. **107**, 252301 (2011).
[10] E. Richardson *et al.* (PHENIX Collaboration), PoS **QNP2012**, 146 (2012).
[11] G. Aad *et al.* (ATLAS Collaboration, Phys. Rev. C **86**, 014907 (2012).
[12] H. Petersen, G.-Y. Qin, S. A. Bass, and B. Muller, Phys. Rev. C **82**, 041901 (2010).
[13] G.-Y. Qin, H. Petersen, S. A. Bass, and B. Muller, Phys. Rev. C **82**, 064903 (2010).
[14] H. Holopainen, H. Niemi, and K. J. Eskola, Phys. Rev. C **83**, 034901 (2011).
[15] B. Schenke, S. Jeon, and C. Gale, Phys. Rev. C **85**, 024901 (2012).
[16] C. Gale, S. Jeon, B. Schenke, P. Tribedy, and R. Venugopalan, Phys. Rev. Lett. **110**, 012302 (2013).
[17] L. Bravina, B. Brusheim Johansson, G. K. Eyyubova, V. Korotkikh, I. Lokhtin *et al.*, Eur. Phys. J. C **74**, 2807 (2014).
[18] B. Abelev *et al.* (ALICE Collaboration), Phys. Lett. B **719**, 18 (2013).
[19] S. Chatrchyan *et al.* (CMS Collaboration), J. High Energy Phys. 02 (2014) 088.
[20] L. P. Csernai, J. I. Kapusta, and L. D. McLerran, Phys. Rev. Lett. **97**, 152303 (2006).
[21] R. A. Lacey, N. Ajitanand, J. Alexander, P. Chung, W. Holzmann *et al.*, Phys. Rev. Lett. **98**, 092301 (2007).
[22] S. Plumari, V. Greco, and L. P. Csernai, arXiv:1304.6566.
[23] S. Plumari, V. Greco, and L. P. Csernai, Nuovo Cim. **C037**, 68 (2014).
[24] M. Prakash, M. Prakash, R. Venugopalan, and G. Welke, Phys. Rep. **227**, 321 (1993).
[25] J.-W. Chen, Y.-H. Li, Y.-F. Liu, and E. Nakano, Phys. Rev. D **76**, 114011 (2007).
[26] H. B. Meyer, Phys. Rev. D **76**, 101701 (2007).
[27] S. K. Das and Jan-e Alam, Phys. Rev. D **83**, 114011 (2011).
[28] S. Plumari, W. M. Alberico, V. Greco, and C. Ratti, Phys. Rev. D **84**, 094004 (2011).
[29] A. Nakamura and S. Sakai, Phys. Rev. Lett. **94**, 072305 (2005).
[30] S. Plumari, A. Puglisi, M. Colonna, F. Scardina, and V. Greco, J. Phys.: Conf. Ser. **420**, 012029 (2013).
[31] S. Plumari, A. Puglisi, F. Scardina, and V. Greco, Phys. Rev. C **86**, 054902 (2012).
[32] M. Ruggieri, F. Scardina, S. Plumari, and V. Greco, Phys. Lett. B **727**, 177 (2013).
[33] M. Ruggieri, F. Scardina, S. Plumari, and V. Greco, Phys. Rev. C **89**, 054914 (2014).
[34] Z. Xu and C. Greiner, Phys. Rev. C **71**, 064901 (2005).
[35] S. Plumari, G. L. Guardo, V. Greco, and J.-Y. Ollitrault, Nucl. Phys. A **941**, 87 (2015).
[36] B. Zhang, M. Gyulassy, and C. M. Ko, Phys. Lett. B **455**, 45 (1999).
[37] D. Molnar and M. Gyulassy, Nucl. Phys. A **697**, 495 (2002).
[38] V. Greco, M. Colonna, M. Di Toro, and G. Ferini, Prog. Part. Nucl. Phys. **62**, 562 (2009).
[39] S. Plumari, V. Baran, M. Di Toro, G. Ferini, and V. Greco, Phys. Lett. B **689**, 18 (2010).
[40] N. Demir and S. A. Bass, Phys. Rev. Lett. **102**, 172302 (2009).
[41] V. Greco, C. M. Ko, and P. Levai, Phys. Rev. Lett. **90**, 202302 (2003).
[42] V. Greco, C. M. Ko, and P. Levai, Phys. Rev. C **68**, 034904 (2003).
[43] B. H. Alver, C. Gombeaud, M. Luzum, and J.-Y. Ollitrault, Phys. Rev. C **82**, 034913 (2010).
[44] C. Gombeaud and J.-Y. Ollitrault, Phys. Rev. C **77**, 054904 (2008).
[45] H. Niemi, G. S. Denicol, P. Huovinen, E. Molnar, and D. H. Rischke, Phys. Rev. C **86**, 014909 (2012).
[46] Y. Hatta, J. Noronha, G. Torrieri, and B.-W. Xiao, Phys. Rev. D **90**, 074026 (2014).
[47] F. G. Gardim, F. Grassi, M. Luzum, and J.-Y. Ollitrault, Phys. Rev. C **85**, 024908 (2012).
[48] A. K. Chaudhuri, M. R. Haque, V. Roy, and B. Mohanty, Phys. Rev. C **87**, 034907 (2013).
[49] H. Niemi, G. S. Denicol, H. Holopainen, and P. Huovinen, Phys. Rev. C **87**, 054901 (2013).
[50] G. Aad *et al.* (ATLAS Collaboration), J. High Energy Phys. 11(2013)183.